scientific reports

Check for updates

OPEN

Lateral flow assay sensitivity and signal enhancement via laser μ-machined constrains in nitrocellulose membrane

Gazy Khatmi[1✉], Tomas Klinavičius[2], Martynas Simanavičius[4], Laimis Silimavičius[3,4], Asta Tamulevičienė[1,2], Agnė Rimkutė[4], Indrė Kučinskaitė-Kodzė[4], Gintautas Gylys[3] & Tomas Tamulevičius[1,2✉]

Lateral flow assay (LFA) is a handful diagnostic technology that can identify severe acute respiratory syndrome coronavirus 2 (SARS-CoV-2) and other common respiratory viruses in one strip, which can be tested at the point-of-care without the need for equipment or skilled personnel outside the laboratory. Although its simplicity and practicality make it an appealing solution, it remains a grand challenge to substantially enhance the colorimetric LFA sensitivity. In this work, we present a straightforward approach to enhance the sensitivity of LFA by imposing the flow constraints in nitrocellulose (NC) membranes via a number of vertical femtosecond laser micromachined microchannels which is important for prolonged specific binding interactions. Porous NC membrane surfaces were structured with different widths and densities μ-channels employing a second harmonic of the Yb:KGW femtosecond laser and sample XYZ translation over a microscope objective-focused laser beam. The influence of the microchannel parameters on the vertical wicking speed was evaluated from the video recordings. The obtained results indicated that μ-channel length, width, and density in NC membranes controllably increased the immunological reaction time between the analyte and the labeled antibody by 950%. Image analysis of the colorimetric indicators confirmed that the flow rate delaying strategy enhanced the signal sensitives by 40% compared with pristine NC LFA.

Keywords Lateral flow assay, Nitrocellulose, M-channels, Laser μ-machining, Reaction time, Calorimetric sensing, Signal enhancement, SARS-CoV-2

On the verge of viral disease outbreaks effective diagnostic methods are of paramount importance. Point-of-care (PoC) diagnostic instruments as rapid diagnostic tests are expected to possess the following attributes: real-time connectivity, ease of specimen collection and environmental friendliness, affordability, sensitivity, specificity, user-friendliness, rapidity, robustness, equipment independence, and accessibility for end-users which was abbreviated as REASSURED criteria[1]. Even though many accurate, reliable, and highly sensitive laboratory methods can be used at the single-cell level such as polymerase chain reaction (PCR), enzyme-linked immunosorbent assay (ELISA), flow cytometry, and Raman spectroscopy, these methods do not fully meet REASSURED criteria as they are costly, time-consuming or are not easy to use and interpret the results[2]. Over nearly the past two decades, the PoC diagnostic methods have made significant progress toward meeting the outlined criteria. In particular, lateral flow assays (LFAs) have emerged as a prominent and popular solution due to their simplicity, speed, portability, affordability, a wide variety of applications, comparable accuracy, shelf stability, and ease of use[3].

Currently, LFAs serve as the most common PoC sensors for diagnosing viruses (human immunodeficiency virus (HIV), hepatitis, severe acute respiratory syndrome coronavirus 2 (SARS-CoV-2)[3]), bacteria (*streptococcus*, *E. coli*), and parasites (malaria[4]) caused infections. They are widely used for determining medical conditions (pregnancy testing and cardiac markers), environmental monitoring (pesticides and heavy metals[5]), food safety applications (such as allergens and pathogens[6]), and cancer markers[7] (prostate-specific antigens, alpha-fetoproteins[8]).

[1]Department of Physics, Kaunas University of Technology, Kaunas, Lithuania. [2]Institute of Materials Science, Kaunas University of Technology, Kaunas, Lithuania. [3]UAB Sanpharm, Vilnius, Lithuania. [4]Institute of Biotechnology, Life Sciences Center, Vilnius University, Vilnius, Lithuania. ✉email: gazy.khatmi@ktu.edu; tomas.tamulevicius@ktu.lt

LFA traditionally consists of a sample pad, conjugate pad, nitrocellulose (NC) membrane, polyvinyl chloride backing card, and absorbent pad (see supplementary Fig. S1). Commercially, the whole assembly is embedded into a housing chamber to improve its usability. In most cases, the LFA colorimetric visual detection is based on the read appearance of gold nanoparticles (Au NPs) which is governed by the dimension and material-related localized surface plasmon resonance (LSPR). The fundamental principles and methodologies of traditional LFAs have been extensively discussed in various scholarly articles and training manuals and will not be discussed in more detail[9]. Whereas this study is focused on laser modified NC paper-based substrate which is the backbone of LFAs enabling low-cost and sustainable manufacturing.

The NC membrane is a microporous material that allows for capillary forces to drive the fluid flow through the test strips where the analytes are detected via specific reactions. The natural capillary action (also known as wicking) in NC eliminates the need for external pumps or complex microfluidic systems. Porous NC matrix provides equipment-free passive microfluidics at the same time providing a biocompatible scaffold that is well-suited for facilitating essential antibodies and antigens biointeractions. Additionally, the flexibility of paper substrates allows for the development of diverse nano-biosensing designs and strategies, e.g., barriers, and constrictions[9]. The most recent research in LFAs concentrates on improving the limit of detection (LoD) and sensitivity[10] as well as multiplexing capabilities for detecting multiple analytes from a single sample[11].

Although LFAs exhibit significant versatility, their use is constrained to mainly qualitative analysis and detection of analytes with relatively high 0.01 mg/mL concentrations. The most significant limitation of traditional LFAs is their batch-to-batch consistency[12] and that are not optimally designed for quantitative measurements or the analyte presence identification at extremely low concentrations as 0.1 ng/mL or fg/mL[13]. It is caused by the interconnected and time-dependent physical (analyte transport dynamics), chemical (reaction kinetics), and optical (signal generation) properties and processes taking place in the LFAs[13]. To overcome these constraints, numerous strategies have been employed to enhance the sensitivity and specificity of LFAs to achieve more precise and superior PoC diagnostics. State-of-the-art improvements to LFA sensitivity can be categorized into three groups of approaches including (i) sample pretreatment, (ii) the change of flow rate, and (iii) the evolution of labels. The first group deals with isothermal nucleic acid amplification and sample enrichment variations. The second one investigated in this work is based on blocking the analyte flow or NC membrane size variation. The last group combines the development of new colorimetric methods and related nanomaterials along with new optical detection methods including laser readout[14], Raman spectroscopy[15], and others[16].

To overcome these constraints, numerous strategies have been employed to enhance the sensitivity and specificity of LFAs to achieve more precise and superior PoC diagnostics. Local control of the lateral flow speed[10] influences the reaction-specific kinetics resulting in the color intensity changes at the detection site. Flow rate can affect reagent dissolution and mixing, as well as reaction effectiveness, and ultimately impact the specific binding (SB) and nonspecific binding (NSB) events, which, in turn, determine the sensitivity and specificity of the assay. Different approaches for controlling the analyte flow and eventually reaction kinetics were tested and can be categorized into chemical and geometrical modification.

Feng Xu et al. slowed down the flow by incorporating a salt barrier. It was found that adding a saline barrier to the membrane before the test region expedited the hybridization reaction attaining a tenfold enhancement sensitivity but at the expense of reduced flow velocity and an extended assay time[17]. Alternatively, Rivas et al. implemented wax pillars on the NC surface to create a delay in the flow and induce pseudo turbulences in the capillary flow. Their approach led to a 3-fold increase in sensitivity for human immunoglobulin G (HigG) detection, compared to the traditional LFA method[18]. Cellulose nanofibers can also be used to modify membranes by changing the properties of the NC membrane to enhance the biomolecule adsorption ability boosting detection sensitivity by 20-fold[19]. Cellulose nanofibers were also reported to bring the captured molecules closer to the surface, thus increasing the colorimetric intensity of the captured labels by 36.5%[21]. Yew et al. utilized electrospinning to deposit polycaprolactone (PCL) nanofibers creating a hydrophobic region on the NC membrane and decreasing the flow rate from 0.35 mm/s to 0.29 mm/s[20]. A theoretical and experimental study by Jia et al. suggested the exploitation of heterogeneous porosity NC membranes with denser NC at the test line of 1.5 μm porosity and sparser in the rest of the membrane length of 24 μm[21].

In contrast, Katis et al. have devised a method to decrease the width of the Test line from 5 to 1 mm. A laser was employed to induce the polymerization of a specific pattern on the NC membrane. By constraining the flow route, a simultaneous augmentation in both the duration of flow and the concentration of the reagents was achieved resulting in a significant 30-fold increase in sensitivity for detecting C-reactive protein. The laser micromachining process is cost-effective and is favorable when compared to alternative patterning techniques like photolithography[22].

Several studies have explored LFA membrane modification utilizing laser-based techniques. Notably, Bikkarolla et al. pioneered a method to laser-pattern NC membranes with CO_2 to create narrow microchannels, enhancing fluid flow control. This approach significantly improves sensitivity and lowers the limit of detection (LoD) by increasing the reaction time between antigens and capture antibodies. Microchannels as narrow as 0.5 mm achieved a ninefold sensitivity improvement and a 6.6-fold reduction in LoD compared to traditional LFAs to 7.5 μIU/ml, making them effective for clinical thyroid-stimulating hormone (TSH) level detection[23]. Modha et al. utilized CO_2 laser-ablated grooves to accelerate wicking speeds on paper. Grooves were ablated with different widths, channel openings, and center-to-center spacing, and wicking highlights the significance of the backing tape and suggests the use of 0.75 mm spaced channels[24]. Sumantakul et al. introduced a CO_2 laser ablation method to fabricate two-dimensional NC-based microfluidic devices, achieving fluid barrier widths of 117 ± 11 μm and channel widths of 81 ± 11 μm. These devices demonstrated superior sensitivity and reduced reagent consumption. Katis et al. utilized direct laser writing in NC membrane with photopolymer to impose constraints and focus the analyte flow into a narrower detection zone, increasing its local concentration and improving sensitivity by 62x and its LoD by 30x when compared to standard LFAs[22].

Continuous wave and pulsed laser of longer pulse length might deteriorate the pore structure and therefore properties of the NC membranes in the vicinity of the laser beam spot imposing significant heat affected zones (HAZ) whereas picosecond and femtosecond pulse length lasers provide "cold" ablation with minimal HAZ[25]. Hecht et al. developed a process using ultrashort laser pulses to integrate fluidic networks in NC membranes, achieving barrier and channel widths of 100 μm and 300–600 μm. They successfully demonstrated a multi-parametric lateral flow test detecting human chorionic gonadotropin (hCG) in multiple channels[25]. As demonstrated in our previous research, Khatmi et al. achieved similar enhancement in fs-laser ablated commercial LFAs by extending the migration duration across the test line from 37 s for a pristine sample to 380 s in laser-structured LFAs, therefore reducing the analyte wicking velocity from 0.2 to 0.048 mm/s and the flow rate from 2.7 to 0.025 μl/s. Furthermore, the colorimetric signal intensity was enhanced by 30% in LFAs featuring 30 μm wide μ channels[26,27].

The ability to control and influence lateral flow speed on the reaction kinetics and binding events provides a foundation for exploring how reactants such as analytes, labeled detection particles (like Au NPs), and various buffer components travel through the NC membrane. In LFAs, SB interactions are targeted to occur at designated test and control lines. This transport within the membrane is governed by mass transfer mechanisms including advection, diffusion, and dispersion. Advection is the primary mechanism for the initial movement of reactants from the sample application point toward the test and control lines. It involves the transport of substances by the bulk movement of a fluid - a liquid analyte sample like blood, serum, or saliva—that carries the reactants through the membrane via capillary action. The directional flow, influenced by the local NC properties, such as flow rate adjustments, significantly affects how and where reactants move within the assay setup. Diffusion, although slower than advection, plays a crucial role in distributing reactants within the membrane, particularly across its width. This ensures that reactants evenly interact with the receptors on the test line, crucial for achieving consistent assay results. Lastly, dispersion, which can be seen as a combination of advection and diffusion, occurs due to variations in flow velocity within the porous structure of the NC membrane. This effect leads to a broadening of the reactant front, enhancing interaction with line receptors but potentially decreasing the sharpness of the detection lines. Understanding these mechanisms helps in refining LFA design and execution, ultimately improving diagnostic accuracy and reliability[28].

The kinetics of transport and immunological reaction are characterized by the Péclet number (Pe) and the Damköhler number (Da), respectively[9]. Where The Péclet number is a dimensionless number that characterizes the relative importance of advective (or convective) transport to diffusive transport. The Damköhler number is a dimensionless number that compares the chemical reaction rate to the rate of transport processes (such as diffusion). In LFAs, a high Pe ($\gg$1) indicates that advection (fluid flow) significantly contributes to the Au NPs transport towards the test site, compared to diffusion. This is important for ensuring that the Au NPs can reach the test site in a timely manner. A low Da($\ll$1) indicates that the reaction rate (e.g., the binding of Au NPs to target molecules at the test site) is the limiting step, not the transport of Au NPs to the site. This could imply that enhancing the reaction kinetics, for example, by increasing the affinity of the Au NPs for the target or optimizing the test site conditions, could improve the assay's performance[9].

The advective flux depends on the velocity of the fluids flowing inside the LFA membrane (v), the pore size of the NC membrane (S), and the diffusivity of the molecules (D) (see Table S1 for details). The reaction rate depends on the concentration of capture molecules in the test region (C_e), the forward reaction rate constant of the single antibody-antigen immunoreaction (K_{on}). Typical parameter values from the literature are summarized in Table S2.

LFAs are intrinsically limited by the reaction rate, and, thus, improving the reaction efficiency is the most critical step toward maximizing SB and boosting the sensitivity of LFAs. The diffusion rate limits the transport of molecules and labels, and the surface reaction rate limits the surface reaction. Increasing reaction efficiency can be accomplished by increasing the reaction rate where the slowing down of the lateral flow increases the reactant concentration and prolongs the reaction time[10].

Among the most important reasons for the poorer sensitivity of LFAs in comparison to other standard laboratory tests, such as ELISA, is that they do not provide as much time for specific binding of biorecognition receptors to antigens or target markers. This is due to the inherent capillary effect of NC, which creates a unidirectional flow of the liquid solution at a constant value across the membrane. The investigated reaction kinetics are associated with forming the conjugation/antigen/captured antibody ternary (sandwich ternary). Liang et al. observed that sandwich ternaries form more slowly when a conjugated label is first used to bind the antigen and then a capture antibody is added sequentially[29]. Thus, the LoD for malarial protein on a sequential flow was reported to be 4 to 10 times lower than that on a premixed flow[29]. Therefore, the goals of optimizing the assay kinetics are to (i) maximize SB and (ii) minimize NSB. Quantitative assay optimization can be achieved by maximizing the signal-to-noise ratio (SB/NSB)[10].

Several studies have been conducted on improving reaction kinetics. At least two methods were reported for reducing the flow rate in LFAs: modifying NC chemically and changing the geometry of the components. Feng Xu et al. slowed down the flow by incorporating a salt barrier. It was found that adding a saline barrier to the membrane before the test region expedited the hybridization reaction attaining a tenfold enhancement sensitivity but at the expense of reduced flow velocity and an extended assay time[17]. Cellulose nanofibers can also be used to modify membranes by changing the properties of the NC membrane to enhance the biomolecule adsorption ability boosting detection sensitivity by 20-fold[19]. Cellulose nanofibers were also reported to bring the captured molecules closer to the surface, thus increasing the colorimetric intensity of the captured labels by 36.5%[21]. Yew et al. utilized electrospinning to deposit polycaprolactone (PCL) nanofibers creating a hydrophobic region on NC membrane and decreasing the flow rate from 0.35 to 0.29 mm/s[20]. Alternatively, Rivas et al. implemented wax pillars on the NC surface to create a delay in the flow and induce pseudo turbulences in the capillary flow.

Their approach led to a 3-fold increase in sensitivity for human immunoglobulin G (HigG) detection, compared to the traditional LFA method[18].

In contrast, Katis et al. have devised a method to decrease the width of the Test line from 5 to 1 mm. A laser was employed to induce the polymerization of a specific pattern on the NC membrane. By constraining the flow route, a simultaneous augmentation in both the duration of flow and the concentration of the reagents was achieved resulting in a significant 30-fold increase in sensitivity for detecting C-reactive protein. The laser micromachining process is cost-effective and is favorable when compared to alternative patterning techniques like photolithography[22].

To summarize, the local lased modification imposing flow control influences assay kinetics and is a critical step in improving LFA performance, which has the potential to increase sensitivity by several orders of magnitude. Flow speed control enables reaction rate control, ensures reactant concentration, prolongs the overall reaction duration, and augments the number of captured labels in the test region. It ultimately impacts the sensitivity and accuracy of the assay. By locally regulating the lateral flow speed, one can optimize the conditions for analyte detection, ensuring the necessary reaction durations. This fine-tuning of reaction kinetics directly influences the intensity of color change at the detection site, which is crucial for accurate target analyte quantification. Moreover, restraining local lateral flow speed allows for better control over the concentration of reactants along the flow path, leading to improved reproducibility and reliability of results. Overall, this strategy enhances the performance of LFAs by maximizing sensitivity, specificity, and consistency in analyte detection[30].

In this work, a straightforward approach for delaying the reaction time and constraining the analyte flow in NC membrane by a varying number of parallel vertical μ-channels imposed employing femtosecond laser μ-machining was proposed. It was demonstrated that μ-channel density, width, and length can controllably constrain the analyte flow. Local delay of the flow by 950% resulted in boosting the immunoreaction rate between antigens and antibodies and increasing the number of captured labels. The colorimetric test line intensity readout of the SARS-CoV-2 analyte improved by 40% at defined μ-channel geometries.

Results and discussion
Ablation threshold of the NC membranes

A porous NC membrane holds inherent surface inhomogeneities in the micron scale and that imposes some challenges for laser ablation at certain resolution. Due to these material variations, laser ablation leads to some variability in ablated hole diameter and depths based on local porosity within the focal volume. For making precise microchannels in the NC surface with minimal damage to the NC membrane and without reaching the polyvinyl chloride backing card it was necessary to determine the laser ablation threshold fluence (F_{th}). Moreover, the F_{th} is an important material characteristic that can be applied in planning future experiments. It was obtained from a dedicated experiment where the second harmonic of Yb: KGW femtosecond laser (Fig. 1a) pulse energy was varied from 13 to 33 nJ and the number of pulses was varied from 10 to 100.

By analyzing the relationship between the laser fluence (F_{th}) and SEM-measured hole diameter the fluence for 10 and 100 pulses was obtained at 170 mJ/cm² and 89 mJ/cm², respectively (Fig. 2a). The ablated crater diameter ended up being bigger than the diffraction-limited spot size because the material is porous. Similar findings were observed in[31]. Hecht et al., conducted a similar experiment where a pulse energy of 0.882 μJ was required for the CN95 ablation with a shorter pulse length femtosecond laser but it was obtained for the moving beam configuration with a f-Theta lens having 12 μm spot size[25]. Skordoulis, involved the use of a CO_2 laser, with ablation thresholds reported at 3.0 and 4.1 J/cm². A moving beam configuration with 24 cm focal length optics was used in conjunction with an iris diaphragm to ablate the target[32].
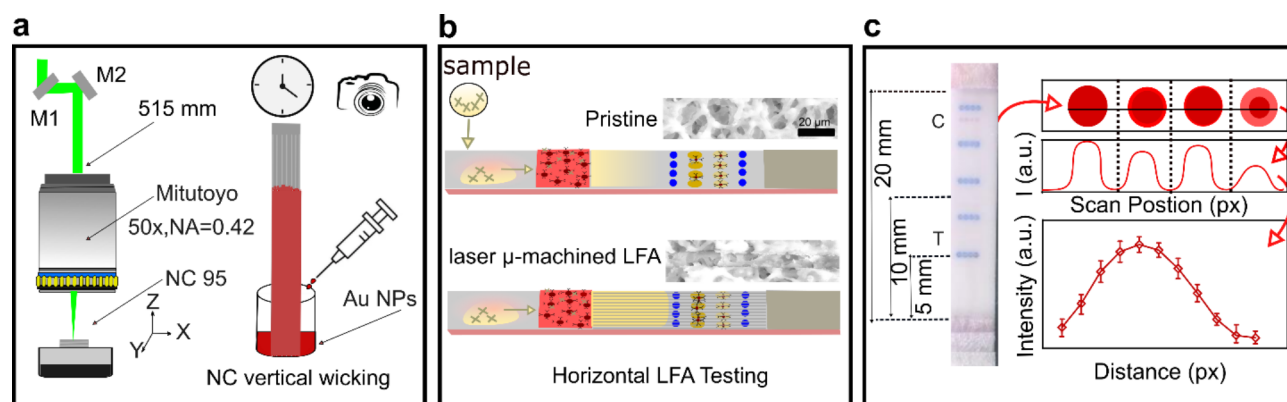
Fig. 1. Schematic illustration of the experimental approach. (**a**) Laser μ-machining process used for structuring NC membrane employing the second harmonic beam delivered by mirrors. Vertical wicking experiment setup for determining the μ-channel influence on the capillary flow rate. (**b**) Horizontal LFA testing principle of pristine and laser processed LFA prototypes. Inset depicts original and laser affected NC membrane porosities. (**c**) Typical LFA test image and its automated sensitivity and signal enhancement analysis process from color images of test ("T") and control ("C") dotted lines averaging the intensity of the four dots.
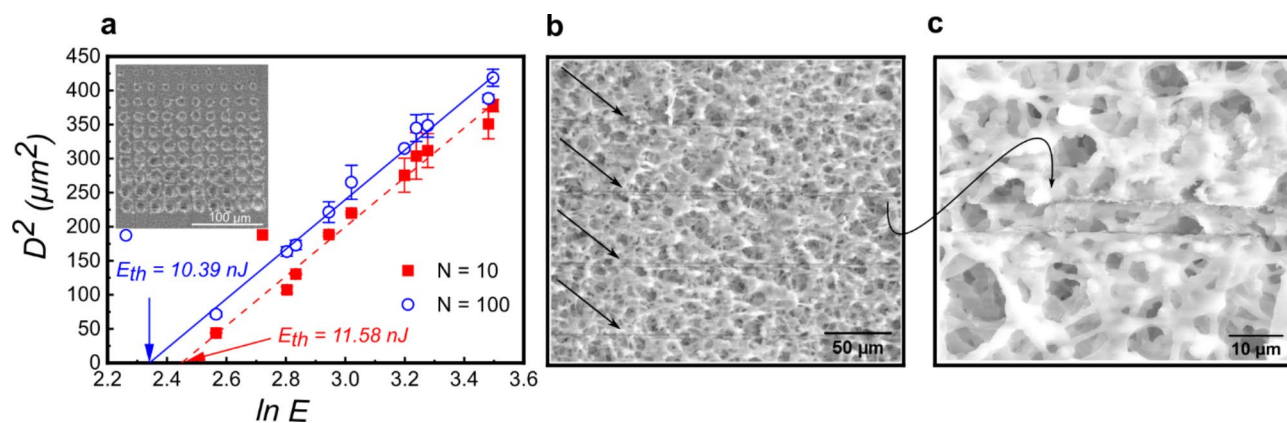
Fig. 2. NC membrane ablation threshold determination. (**a**) The average squared crater diameter vs. applied logarithm of applied energy per pulse using $N = 10$ and 100 pulses. The error bars represent one standard deviation from three diameter measurements. The inset depicts an fs-laser ablated membrane SEM micrograph with different energy and the number of pulses. (**b**) SEM micrograph of multiple laser µ-machined channels indicated by arrows. (**c**) Close-up SEM view of a single 5 µm width µ-channel.

| Parameter	Ablation	
	Fast	Slow
Pulse repetition, f (kHz)	200	40
Average power, P (mW)	3.7	2.5
Pulse energy, E (nJ)	18.5	65.5
Scan speed, v (mm/s)	5	1
Pulse density (pulses/mm)	40,000	
Laser fluence, F (J/cm^2)	0.41	1.38
Ablation threshold F_{th} (J/cm^2)	0.089	

Table 1. Typical laser parameters used for the ablation of NC membranes.

We observed a decrease in the threshold fluence with an increasing number of pulses. Specifically, the threshold fluence (F_{th}) was found to be 4.1 mJ/cm^2 for 10 pulses and 3.6 mJ/cm^2 for 100 pulses, respectively (Fig. 2a). This behavior is well-documented and is typically explained by the incubation effect, which has been studied across a wide range of materials, including semiconductors, metals, dielectrics, ceramics, and polymers[33].

After some laser ablation trials varying pulse energy, scanning speed, and pulse density two prospective parameter datasets were identified with identical pulse densities where decrease in scanning speed and pulse repetition was compensated by increased energy per pulse that were termed "Fast" and "Slow" as summarized in Table 1. Latter ablation conditions resulted in different ablation depth and line edge roughness as seen in Fig. 3. It was obtained that under slow conditions the original membrane structure is intact and does not change the porosity. By using this more precise and controlled cutting method, we can avoid irregularities such as zigzags seen in the case of "Fast" cutting (Fig. 3bottom µ-channel). The "Slow" ablation provides better-defined channels that reduce flow turbulence and resistance caused by uneven surfaces[25], despite longer µ-machining duration. Eventually, it might lead to better-controlled fluid flow therefore "Slow" (Fig. 2b,c) ablation conditions were preferred in the following investigations discussed in this work.

Characterization of gold nanoparticles

Aiming to mimic the LFA operation and wicking restriction in laser µ-structured NC membrane gold nanoparticle colloids were chemically synthesized. The synthesis of AuNPs was achieved using trisodium citrate as the reducing agent for Au NPs. The reduction reactions were conducted under carefully optimized conditions including controlled temperature and reaction time to facilitate the nucleation and growth of stable nanoparticles. The colloid had a characteristic pink color (Fig. 4a inset) explained by the LSPR-related Au NP extinction at 530 nm seen in the UV-Vis spectra (Fig. 4a)[34]. The particle shape was close to spherical with the ca. 50 nm average diameter (Fig. 4b).
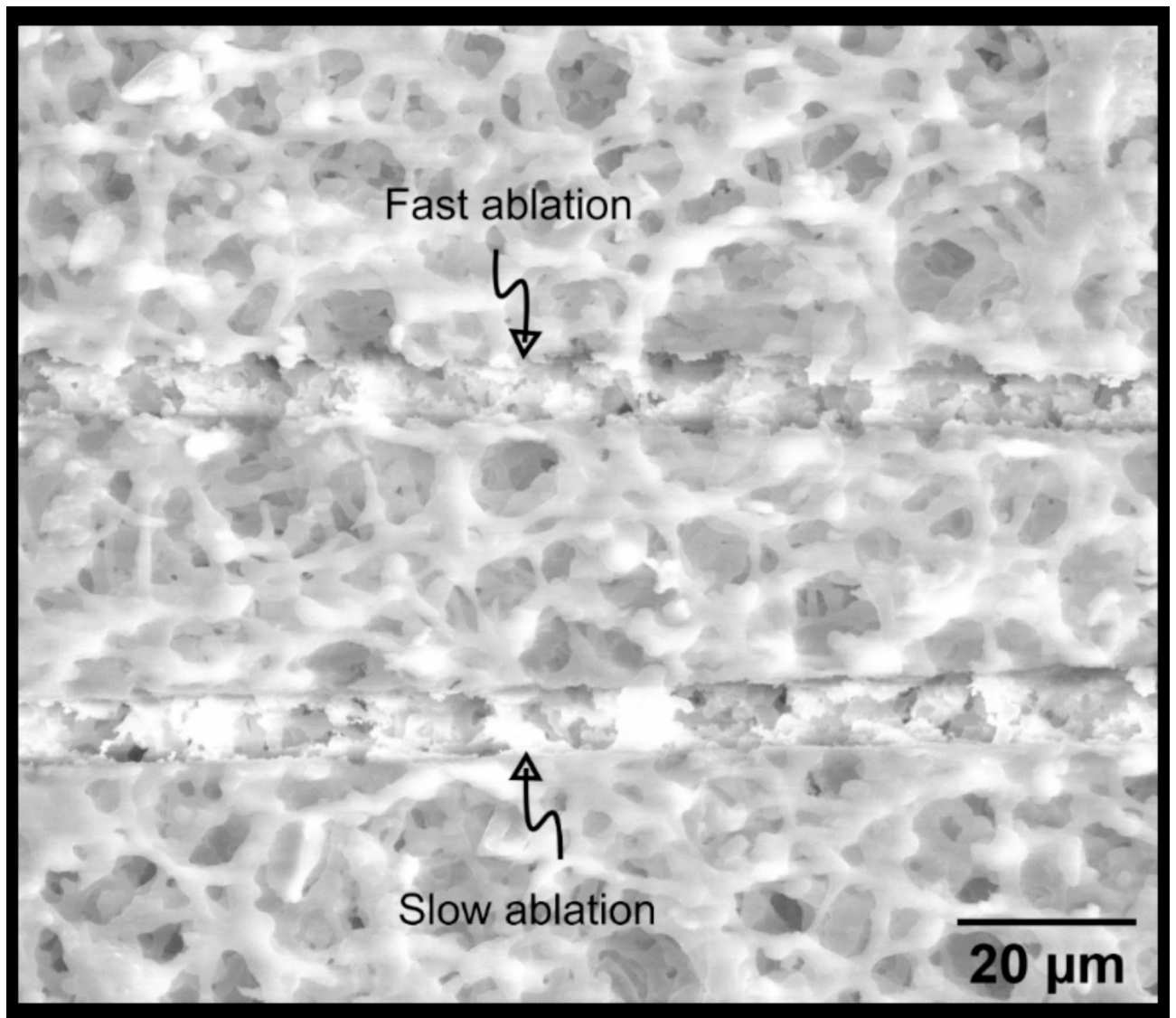
Fig. 3. SEM micrograph of laser-ablated microchannels under two different conditions. The top μ-channel is abated by faster scanning than the bottom one as explained in Table 1.

μ-channel influence on the wicking flow

After selecting the "slow" laser ablation condition parameters (Table 1) the influence of the μ-channel width and length on the Au NP colloid vertical capillary flow (Fig. 1a) over a 20 mm length NC membrane (Fig. 1c) was investigated. The influence of the fs-laser μ-machined channel length and density is depicted in Fig. 5.

The nominal capillary vertical flow duration across a 20 mm long membrane was 40 s. Supplementary Movies S1 and S2 depict camera videos of two typical wicking experiments of pristine and laser-treated NC membranes respectively. After the laser treatment, the wicking across the same length took up to 420 s as seen in Fig. 5. Our study revealed that the laser treatment led to a substantial increase in the nominal flow rate, with the wicking process across the same length taking up to 380 s. It was estimated that the interaction time rose by 950% in comparison to the pristine strip when the μ-channel width was 50 μm and length was 20 mm. Shorter μ-channels of 10 mm and 5 mm length exhibited an increase of at least 600% and 125%, respectively. It was confirmed that varying the width of channels also has a noticeable impact (Fig. 5b) where μ-channels ranging from 5 to 50 μm exhibited a consistent reduction in wicking velocity, decreasing flow speed from 0.13 mm/s to 0.06 mm/s, respectively, when compared to 0.20 mm/s velocity in the unmodified NC.

This represents a significant deviation from previous methodologies, such as the approach by Fei Li et al., where the electrospun polycaprolactone (PCL) on NC membrane resulted in a considerably shorter delay of flow, achieving 28 ± 2% delay for travel a 3.0 cm distance[20].

In comparison to the work by Joong Ho Shin et al., our study resulted in a similar delay compared to the NC membrane under compressive 23.54 MPa pressure which reduced the flow rate and led to a substantially longer time of approximately 11 more minutes for the diluted serum to flow through[35]. Xiao Feng Xu et al.[36], achieved delays of 25%, 75%, and 100% by integrating the sponge shunt after the conjugation pad into LFA and
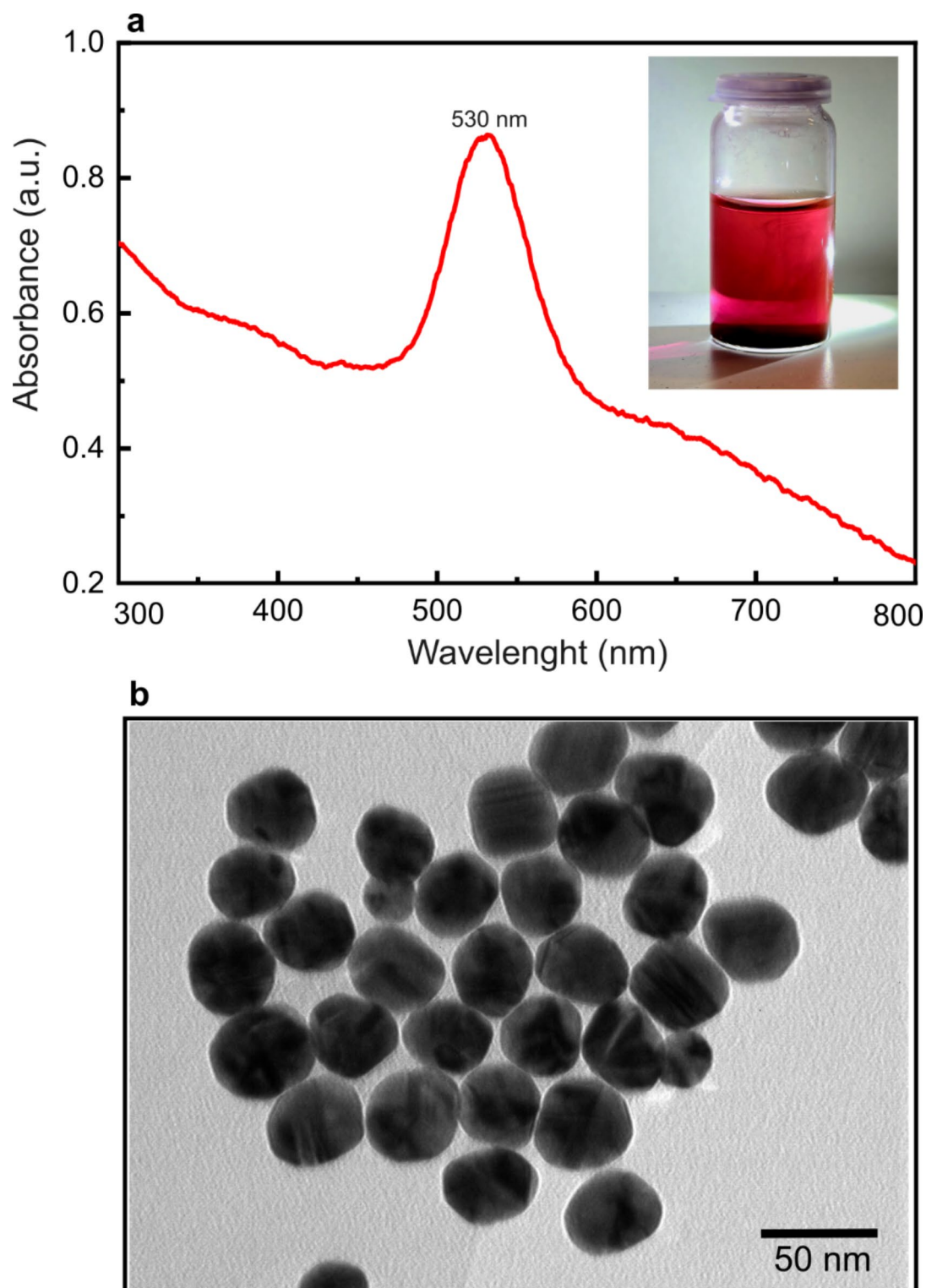
Fig. 4. Characterization of gold NPs. (**a**) The UV-Vis absorbance spectra of AuNPs. The inset depicts the camera image of the gold NPs in the vial. (**b**) A TEM micrograph Au NPs.

varying the thickness, length, and hydrophobicity of the sponge. Arben et al.[37], designed different wax barriers of different widths of 0.01 mm, 0.03 mm, and 0.05 mm and achieved 4 min, 7 min, and 12 min flow delay for lateral flow over 60 mm×3 mm membrane. Zhiqing Xiao et al.[38] developed an easy method to adjust the capillary flow rate on LFA substrates by using tape to cover the surface of substrates and achieved an average flow rate decrease of 61% of the original flow rate on synthetic paper. It is worth mentioning that the role of analyte evaporations was not controlled in this study. Some previous works suggest that evaporation can enhance diffusion[39,40] but
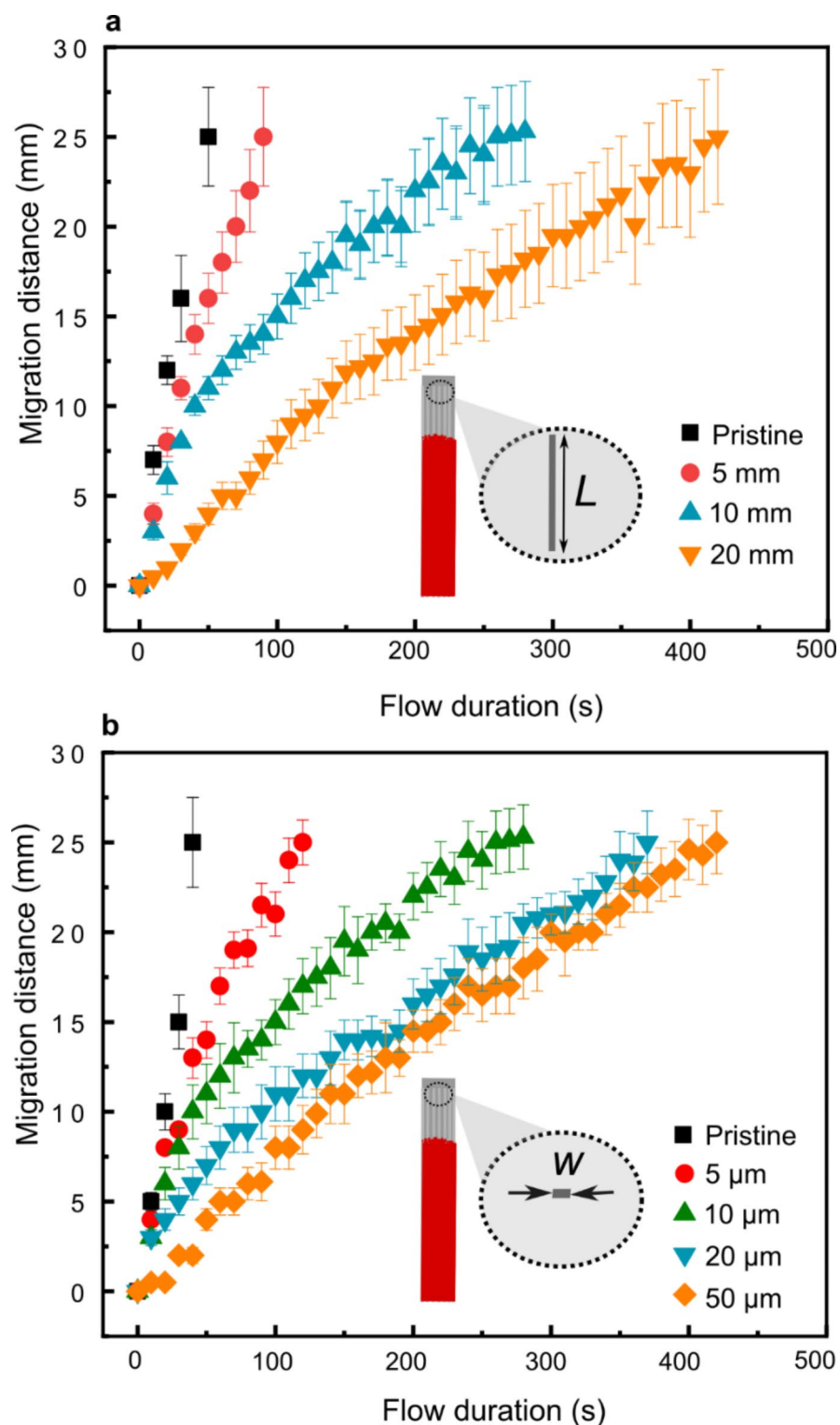
Fig. 5. Migration distance as a function of time for pristine and laser µ-machined NC membranes. The migration distance of the Au NP colloid in NC membrane at different time moments depending on the length (**a**) and width (**b**) of laser ablated µ-channels. The µ-channel density in both cases fills 4 mm of the NC strip and the number of µ-channel depends on their width (gap and spacing are the same). The width in (**a**) is 50 µm and the length in (**b**) is 10 mm.

such experiments should be carried out in the microenvironment[41] whereas here experiments were carried out in standard laboratory conditions. The use of the backing card partially mitigated this issue because it prevented evaporation from one of the membrane surfaces.

μ-channel influence on the SARS-cov-2 detection sensitivity

The experience gained on delaying flows in the laser-processed NC membrane was tested on the multiple respiratory diseases detecting LFA prototype based on the same NC membrane type using SARS-CoV-2 analyte. The LFA contained all the typical LFA components including sample pad, conjugate, and absorbent pads, test, and control lines as shown in Fig. 1b. The blue dotted lines in the diagnostic tests are for coordination and easiness of the automated image readout process. After the testing in some cases, the alignment markers became darker and that is the combined effect of local differences in fs-laser modification, interaction with the assay components, and dye concentration variation. It did not influence the accurateness of the image alignment before the read-out of the assay as explained in Fig. S4. Aiming to distinguish the influence on the colorimetric readout of the laser μ-machined channels, the differently laser-treated LFAs were compared with the pristine LFA sample. The biofunctionalized active area of the test was laser treated with different lengths and density μ-channels employing the identical conditions met in "μ-channel influence on the wicking flow".

After the SARS-CoV-2 analyte was applied to the pristine and laser-structured LFAs their color image was scanned and analyzed automatically using a custom image analysis code as explained in (Fig. 1c). The results of the Test and Control line relative intensities of differently laser-treated LFAs are summarized in Fig. 6. The analyzed images of the Test and Control lines are depicted on the top rows in Fig. 6 together with the peak signal values corresponding to the brightest signal in the middle of the red dots used for colorimetric recognition of the specific binding event below. The averaged signal variation over the four dots widths is depicted in Fig. 7.

Low laser fluence and sparse μ-channels did not affect biofunctionalized areas during the engraving process of the NC membrane.

The SARS-CoV-2 test line intensity increased by 16% for 5 mm length and 50 μm width treated LFA (Fig. 6b, Fig. S3) compared to the pristine test (Fig. 6a). When the channel length was 10 mm, the intensity increased by 21% (Fig. 6c, Fig. S3). The biggest signal was registered for a full strip length modified LFA (20 mm) where the test line signal increased by 40% for the case of widest μ-channels (Fig. 6d, Fig. S3).

In the case of pristine LFA, the difference between the Test and Control lines was minimal because quite a big analyte concentration was applied. The micro structured LFA Test and Control line signal compared to the pristine sample increased in all investigated cases. It was observed that the signal was increasing with the increasing width of the μ-channels despite the overall length of the imposed modifications (Figs. 6 and 7). The SARS-CoV-2 test line intensity increased by 16% for 5 mm length and 50 μm width treated LFA (Fig. 6b) compared to the pristine test (Fig. 6a). When channel length was 10 mm, the intensity increased by 16% (Fig. 6c). The biggest signal was registered for a full strip length modified LFA (20 mm) where the test line signal increased by 40% for the case of widest μ-channels (Fig. 6d).

Low laser fluence and sparse μ-channels did not affect biofunctionalized areas during the engraving process of the NC membrane. Still, slightly higher intensities over the test line were formed for 5 mm μLFA due to the narrow flow paths and slight local decrease of flow velocity (v), as seen in (Fig. 7b). It can be observed that the binding of the AuNPs is more uniform in the case of 50 μm. In the case of 5 μm channel width multiplex LFA has not shown a noticeable difference in the brightness of the test line, as shown in (Fig. 7a–c). In addition, the brightness of the test lines was higher when the length of channels increased as shown in (Figs. 6d and
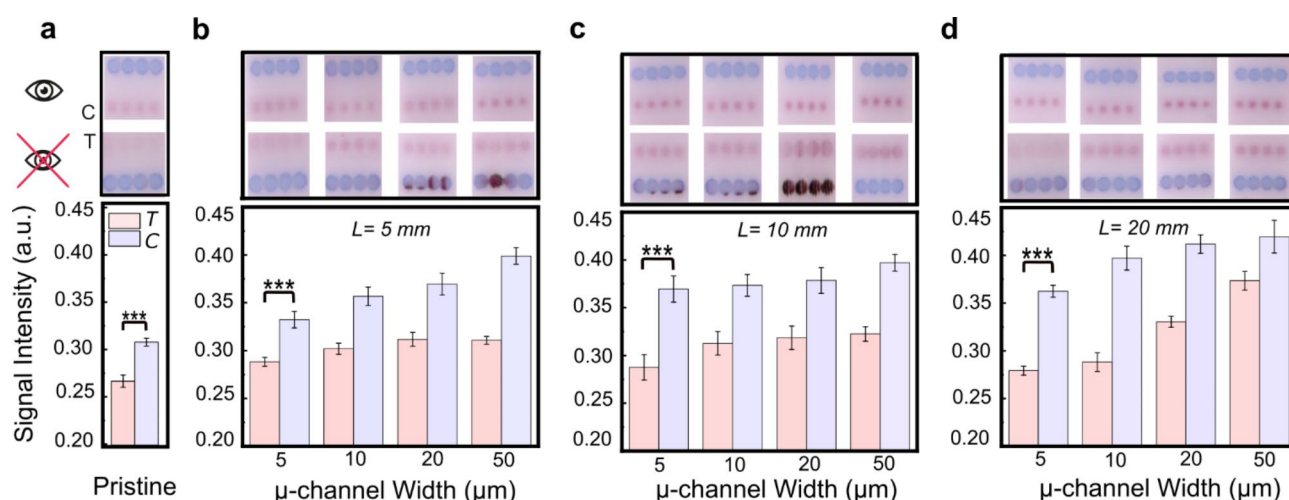
Fig. 6. Maximum response of relative intensity of test ("T") and control ("C") lines as discerned from the camera image analysis after applying SARS-CoV-2 analyte. The signal intensity value is a grayscale amplitude averaged along the four dots. The error bars indicate the standard deviations of the gray-scale values obtained from four individual dots. The reference LFA without laser modification (**a**) and with laser μ-machined microchannel of different lengths 5 mm (**b**), 10 mm (**c**), and 20 mm (**d**).
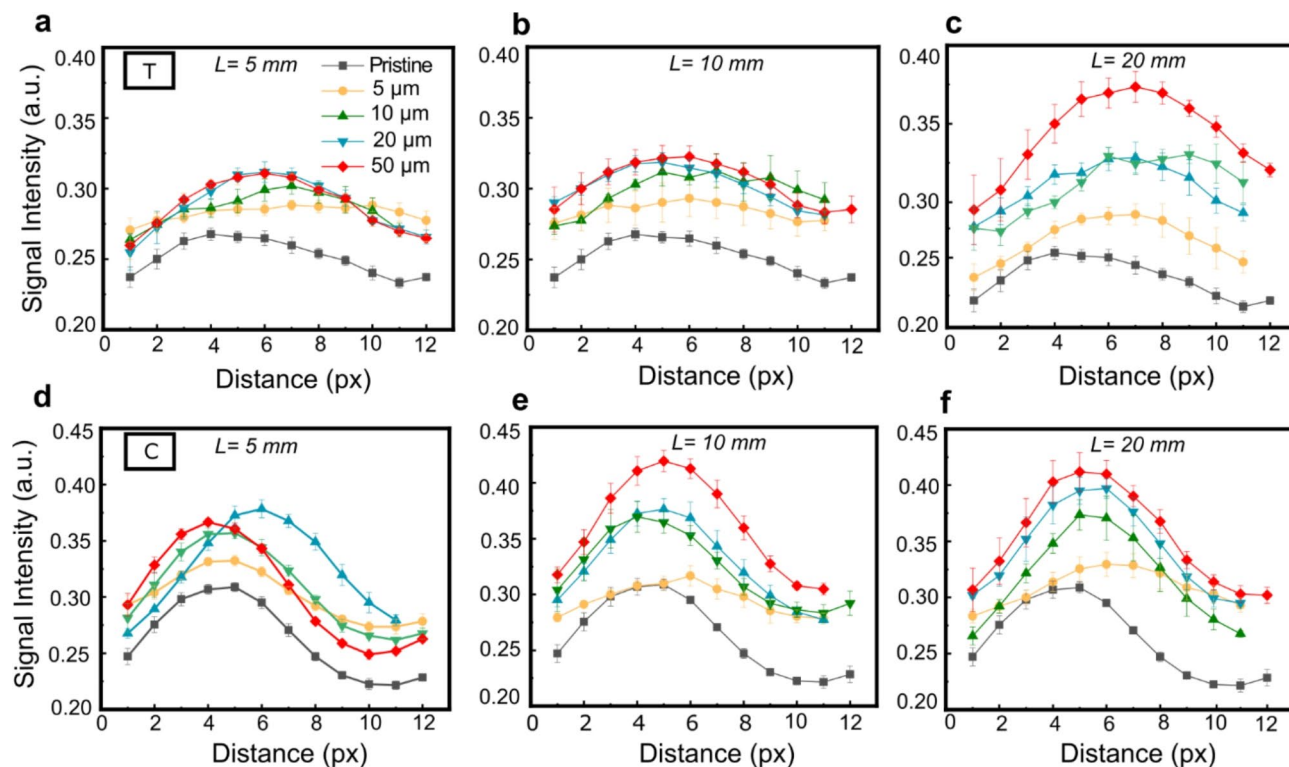
Fig. 7. Pristine and differently laser μ-machined LFA "T" (**a**–**c**) and "C" (**d**–**f**) line image analysis results after applying SARS-CoV-2 analyte. Mean signal intensity was estimated from the automated analysis of the gray-scale value intensities measured along the four dots. The with of the channels is indicated in the legend and the length of the μ-channels was 5 mm (**a**, **d**), 10 mm (**b**,**e**), and 20 mm (**c**,**f**).

7c,f). Similarly, as for the vertical wicking experiments, the LFA results might have been affected by the solvent evaporation as the plastic protective casing[42] was not used for the prototype LFA test but the experiment conditions were identical for all investigated samples.

The results confirmed our initial hypothesis that μ-channel can constrain the Au NP flow velocity (*v*) through NC membrane flow before reaching the test region and increase the time of reaction (*T*). The laser modification increased the ratio of diffusion time to convection time of Au NPs (*Pe*, see Table S1) and decreased the ratio of the refraction flux to diffusion flux (*Da*), which is directly proportional to the reaction rate constant $k'_{on} = n \cdot k_{on}$ for antibody-labeled Au NPs. Where n is an effective number of antibodies per Au NPs with calculated $Pe \gg 1$ (convection-dominated diffusion) and $Da \ll 1$ (diffusion-dominated reaction), thus the reaction was a rate-limiting step to improve Au NP capture. While k_{on} is the forward rate constant for a single antibody-antigen interaction in the NC membrane. The results suggest that significantly lowering and constraining the Au NP flow rate the prolonged reaction time leads to more expressed binding of AuNPs over the Test line.

Experimental/materials and methods
Used materials
The nitrocellulose membranes used for laser treatment influence on wicking experiments in this study were NC 95 (Carl ROTH, Gmbh&CO) with an average pore size of 5 μm. The prototype multiplex respiratory viral diagnostic test "MultiRespiTest" depicted in Fig. S5 was developed by UAB "Sanpharm" (Lithuania). The prototype diagnostic tests could detect specific binding with SARS-CoV-2, Influenza B virus, Human Bocavirus 1, Respiratory Syncytial Virus, Human Parainfluenza Virus 1, Human Parainfluenza Virus 3, and Human Metapneumovirus. Only SARS-CoV-2 analyte was used in this work. To prepare a prototype LFA following materials were used: CN95 nitrocellulose membrane (Sartorius), sample pad (Ahlstrom 1281), conjugate pads (Ahlstrom 6613 and 8950), wicking pad (Ahlstrom 222), backing card (nanoComposix), Potassium phosphate dibasic (Sigma-Aldrich, CAS No. 7758-11-4), Potassium phosphate monobasic (Sigma-Aldrich, CAS No. 7778-77-0), TRIS (Carl-Roth, CAS No. 77-86-1), Hydrochloric acid (Carl-Roth, CAS No. 7647-01-0), Sodium chloride (Carl-Roth, CAS No. 7647-14-5), Bovine serum albumin Fraction V (Carl-Roth, CAS No. 9048-46-8), Triton X-100 (Carl-Roth, CAS No. 9002-93-1), ProClin 300 (Sigma-Aldrich), D-glucose (Carl-Roth), Remazol Brilliant Blue R (Sigma-Aldrich), Sodium carbonate (Carl-Roth, CAS No. 497-19-8), Sodium dodecyl sulfate (SDS, Carl-Roth, CAS No. 151-21-3), Xylene Cyanol FF (Sigma-Aldrich, CAS No. 2650-17-1), Orange G (Sigma-Aldrich, CAS No. 1936-15-8), Bromphenol blue (Carl-Roth, CAS No. 115-39-9), ROTI®PreMix PBS (Carl-Roth). For the detection of SARS-CoV-2 analyte mouse monoclonal antibodies mAb-12B2, mAb-4G6, and mAb-6G11 to SARS-CoV-2 nucleocapsid (N) protein were used (developed in-house) for test dots. For control dots, polyclonal

antibodies Goat Anti-Mouse IgG Fc-UNLB (SouthernBiotech) were used. As SARS-CoV-2 analyte recombinant full-length SARS-CoV-2 rN protein (Baltymas, Lithuania, cat. no. 20-S2N-ScA-F) was used. More experimental details are provided in supplementary information Sect. S2.3.

Methods

Modification of NC membrane by laser µ-machining

The femtosecond laser ablation tests and µ-channels in NC membranes on polyvinyl chloride backing card and prototype LFAs (MultiRespiTest, Sanpharm) were imposed employing a second harmonic of the 290 fs pulse length Yb: KGW femtosecond laser Pharos (Light Conversion, Lithuania) and a second harmonic generator Hiro (Light Conversion, Lithuania) using an XYZ translation stage based workstation FemtoLab (Altechna R&D, Lithuania) which was controlled by the SCA µ-machining software (Altechna R&D, Lithuania) (Fig. 1a). The 515 nm wavelength light was focused with the 0.42 NA, 50× Plan Apo NIR objective (Mitutoyo, Japan). More details on the used laser system can be found elsewhere[43].

The ablation threshold of the NC membrane was determined according to the method proposed by Liu[44] assuming Gaussian intensity distribution within the laser spot. The percussion-ablated array of holes with varied pulse energy (E_p) from 13 to 33 nJ with an increment of ca. 10% and changed number of pulses (N) from 10 to 100 with 10 pulse increments were investigated under a scanning electron microscope. The damaged area of the material was approximated by the diameter (D) which was an average of the hole diameter along two orthogonal orientations. The laser beam waist (w_0) and ablation threshold energy ($E_{th}(N)$) were determined from the slope and x-intercept with the linear regression of the function $D^2 = \ln(E_p)$, respectively[45]

$$D^2 = 2w_0^2\ln(E_p/E_{th}(N)) \tag{1}$$

The laser ablation damage threshold F_{th} is calculated from the obtained waist and threshold energy[44]:

$$F_{th} = 2E_{th}/\pi\, w_0^2 \tag{2}$$

The different lengths µ-channels of 5 mm, 10 mm, and 20 mm were ablated in NC membranes, and LFAs as overlapping lines with 0.001 mm spacing were imposed under two characteristic ablation conditions that were analyzed in more detail as summarized in Table 1. The number of µ-channels per 5 mm NC membranes or LFAs depended on the width of the single µ-channel keeping the gap of the same size. Microchannel widths of 5 µm, 10 µm, 20 µm, and 50 µm were investigated.

Laser-processed NC membranes were analyzed with an environmental field emission gun scanning electron microscope (SEM) Quanta 200 FEG (FEI, Netherlands) operated in the low vacuum mode.

Preparation of aunps

Colloidal gold nanoparticles for wicking experiments were chemically synthesized according to the route described in[34]. In short, the synthesis consists of two steps starting from seed synthesis and the second step of growth of nanoparticles. Seeds were synthesized by heating 150 ml of 2.2 mM sodium citrate solution for 15 min under vigorous stirring. After the solution started to boil, 1 ml of $HAuCl_4$ (25 mM) was injected. The color of the solution changed to soft pink in 10 min. Immediately after the seed synthesis, the reaction was cooled to 90 °C, and 1 ml of $HAuCl_4$ (25 mM) was injected. The solution was left for 30 min stirring heating at 90 °C. This procedure was repeated twice. After that, 55 ml of sample was extracted and 53 ml of water and 2 ml of 60 mM sodium citrate were added to the same vessel. Chemicals were acquired from Sigma Aldrich. This solution was then used as a seed solution, and the process was repeated. The absorbance of the colloid was inspected using UV-Vis-NIR spectrophotometer Avaspec-2048 and combined Deuterium/Halogen lamp light source AvaLight-DHc (Avantes, Netherlands). The 1.5 optical density (OD) colloid was used for the wicking without further dilution. The size of the Au NPs was evaluated from the drop-cast colloid on the transmission electron microscope (TEM) grid employing Tecnai G2 F20 X-TWIN (FEI).

Wicking experiments

The vertical wicking speed of the pristine and laser-treated NC membrane strips of 5 mm width and 20 mm length was inspected by immersing in the 0.5 ml vial (Eppendorf) with 100 µl of the Au NP colloid. The experiments were carried out in air-conditioned laboratory conditions at 20 ± 1 °C temperature and 50 ± 5 relative humidity during the summer period. The smartphone camera was used to record the process. The red color of the Au NP colloid improved the flow visualization and mimicked the actual LFA experiment. The measurement setup is depicted in Fig. 1a. The recorded videos were analyzed every 10 s to measure the solution front position on the NC membrane.

Automated image analysis

The SARS-CoV-2 sample (10 ng/µL of recombinant SARS-CoV-2 nucleocapsid protein (UAB Baltymas, Lithuania) in 100 µL sample buffer) was applied with a pipette on pristine and differently laser-treated LFA prototype tests without casing. After 30 min incubation at laboratory conditions, the LFAs were scanned with a flatbed scanner Perfection V370 Photo (Epson) for further image analysis. The doted color test lines were carefully chosen in the images, and the average intensity values were measured by a dedicated code implemented in MATLAB (MathWorks, CA, USA). The key steps of the region of interest selection and image pretreatment are showcased in Fig. S4. The signal values were evaluated by removing the background noise by calculating the average intensity value for each doted strip. The pixel intensity across the line, originally stored as a full-color RGB, was converted to grayscale. The resulting intensity values were inverted to address a darker color to a

higher intensity value. A slicing location of the affected region was selected manually and a single pixel-wide line passing through all 4 dots of the Test line and Control lines was extracted for further analysis. The originally dotted line was then divided into 4 equal-length segments of 12 pixels. The segments were averaged, and the standard error of the mean was computed for each pixel value, including the maximum value of the average. The Origin 2019b (OriginLab) software was used to analyze the results statistically.

Conclusions

We have proposed an innovative approach to improve the signal sensitivity of colorimetric readout lateral flow assays (LFAs) based on nitrocellulose membranes. It was achieved by imposing microchannels in NC membranes employing femtosecond laser cold ablation. The microchannels delayed the flow rate on the strip thereby increasing reaction time between the analyte and the labeled antibody leading to a more effective formation of the immunocomplex observed as a brighter colorimetric signal. The 50 µm widths µ-channel demonstrated an increase in flow rate delay of 125% and 600% when the channel length was extending over 5 mm and 10 mm, respectively. Moreover, this value reached 950% when the channels extended over all 20 mm lengths of the NC membranes. As a result of this strategy, the sensitivity of the prototype LFA test was increased by 40% for the SARS-CoV-2 analyte compared with the untreated LFA. The proposed method can be extended for further development of the limit of detection and analytical sensitivity in point-of-care diagnostic devices.

Data availability

The authors have no competing interests to declare that are relevant to the content of this article. The datasets generated during and/or analysed during the current study are available from the corresponding authors on reasonable request.

References

1. Mabey, D. et al. Diagnostics for the developing world. *Nat. Rev. Microbiol.* **2**, 231–240. https://doi.org/10.1038/nrmicro841 (2004).
2. Land, K. J., Boeras, D. I., Chen, X. S., Ramsay, A. R. & Peeling, R. W. REASSURED diagnostics to inform disease control strategies, strengthen health systems and improve patient outcomes. *Nat. Microbiol.* **4**, 46–54. https://doi.org/10.1038/s41564-018-0295-3 (2019).
3. Parolo, C. & Merkoçi, A. Paper-based nanobiosensors for diagnostics. *Chem. Soc. Rev.* **42**, 450–457. https://doi.org/10.1039/C2CS35255A (2013).
4. Lin, H. et al. Rapid visual detection of plasmodium using recombinase-aided amplification with lateral flow dipstick assay. *Front. Cell. Infect. Microbiol.* **12**. https://doi.org/10.3389/fcimb.2022.922146 (2022).
5. Srinivasan, S., Ranganathan, V., McConnell, E. M., Murari, B. M. & DeRosa, M. C. Aptamer-based colorimetric and lateral flow assay approaches for the detection of toxic metal ions, thallium(i) and lead(ii). *RSC Adv.* **13**, 20040–20049. https://doi.org/10.1039/D3RA01658G (2023).
6. Shan, S., Lai, W., Xiong, Y., Wei, H. & Xu, H. Novel strategies to enhance lateral flow immunoassay sensitivity for detecting foodborne pathogens. *J. Agric. Food Chem.* **63**, 745–753. https://doi.org/10.1021/jf5046415 (2015).
7. Meng, X. et al. Bimetallic nanozyme: a credible tag for in situ-catalyzed reporter deposition in the lateral flow immunoassay for ultrasensitive cancer diagnosis. *Nano Lett.* https://doi.org/10.1021/acs.nanolett.3c03118 (2023).
8. Mahmoudi, T., de la Guardia, M. & Baradaran, B. Lateral flow assays towards point-of-care cancer detection: a review of current progress and future trends. *TrAC - Trends Anal. Chem.* **125**. https://doi.org/10.1016/j.trac.2020.115842 (2020).
9. Zhan, L. et al. The role of Nanoparticle Design in determining Analytical performance of lateral Flow immunoassays. *Nano Lett.* **17**, 7207–7212. https://doi.org/10.1021/acs.nanolett.7b02302 (2017).
10. Liu, Y., Zhan, L., Qin, Z., Sackrison, J. & Bischof, J. C. Ultrasensitive and highly specific lateral Flow assays for point-of-care diagnosis. *ACS Nano.* **15**, 3593–3611. https://doi.org/10.1021/acsnano.0c10035 (2021).
11. Shen, Y. & Shen, G. Signal-enhanced lateral Flow Immunoassay with Dual Gold Nanoparticle conjugates for the detection of Hepatitis B Surface Antigen. *ACS Omega.* **4**, 5083–5087. https://doi.org/10.1021/acsomega.8b03593 (2019).
12. Soh, J. H., Chan, H. M. & Ying, J. Y. Strategies for developing sensitive and specific nanoparticle-based lateral flow assays as point-of-care diagnostic device. *Nano Today.* **30**. https://doi.org/10.1016/j.nantod.2019.100831 (2020).
13. Bishop, J. D., Hsieh, H. V., Gasperino, D. J. & Weigl, B. H. Sensitivity enhancement in lateral flow assays: a systems perspective. *Lab. Chip.* **19**, 2486–2499. https://doi.org/10.1039/c9lc00104b (2019).
14. Peng, T. et al. Enhancing sensitivity of lateral flow assay with application to SARS-CoV-2. *Appl. Phys. Lett.* **117**. https://doi.org/10.1063/5.0021842 (2020).
15. Xiuli Fu a, Z. C., a, J. Y., a, P. C., b, L. C. & c, J. C. A SERS-based lateral flow assay biosensor for highly sensitive detection of HIV-1 DNA. *Biosens. Bioelectron.* https://doi.org/10.1016/j.bios.2015.11.09 (2016).
16. Deng, Y., Jiang, H., Li, X. & Lv, X. Recent advances in sensitivity enhancement for lateral flow assay. *Microchim. Acta.* **188**. https://doi.org/10.1007/s00604-021-05037-z (2021).
17. He, X. et al. Sensitivity enhancement of nucleic acid lateral Flow assays through a physical-chemical coupling method: Dissoluble saline barriers. *ACS Sens.* **4**, 1691–1700. https://doi.org/10.1021/acssensors.9b00594 (2019).
18. Rivas, L., Medina-Sánchez, M., De La Escosura-Muñiz, A. & Merkoçi, A. Improving sensitivity of gold nanoparticle-based lateral flow assays by using wax-printed pillars as delay barriers of microfluidics. *Lab. Chip.* **14**, 4406–4414. https://doi.org/10.1039/c4lc00972j (2014).
19. Wang, X. et al. Modification of a nitrocellulose membrane with nanofibers for sensitivity enhancement in lateral flow test strips. *RSC Adv.* **11**, 26493–26501. https://doi.org/10.1039/D1RA04369B (2021).
20. Yew, C. H. T., Azari, P., Choi, J. R., Li, F. & Pingguan-Murphy, B. Electrospin-coating of nitrocellulose membrane enhances sensitivity in nucleic acid-based lateral flow assay. *Anal. Chim. Acta.* **1009**, 81–88. https://doi.org/10.1016/j.aca.2018.01.016 (2018).
21. Pengpeng Jia, Z. et al. Performance improvement of lateral flow assay using heterogeneous nitrocellulose membrane with nonuniform pore size. *Int. Commun. Heat Mass Transfer.* https://doi.org/10.1016/j.icheatmasstransfer.2023.106729 (2023).
22. Ioannis, N., Katis, Peijun, J. W., He, R. W., Eason, C. L. & Sones Improved sensitivity and limit-of-detection of lateral flow devices using spatial constrictions of the flow-path. *Biosens. Bioelectron.* **113**, 95–100. https://doi.org/10.1016/j.bios.2018.05.001 (2018).
23. Bikkarolla, S. K. et al. A lateral flow immunoassay with self-sufficient microfluidic system for enhanced detection of thyroid-stimulating hormone. *AIP Adv.* **10**. https://doi.org/10.1063/5.0026047 (2020).

24. Modha, S., Shen, Y., Chamouni, H., Mulchandani, A. & Tsutsui, H. Laser-etched grooves for rapid fluid delivery for a paper-based chemiresistive biosensor. *Biosens. Bioelectron.* **180**. https://doi.org/10.1016/j.bios.2021.113090 (2021).
25. Hecht, L., Van Rossum, D. & Dietzel, A. Femtosecond-laser-structured nitrocellulose membranes for multi-parameter point-of-care tests. *Microelectron. Eng.* **158**, 52–58. https://doi.org/10.1016/j.mee.2016.03.020 (2016).
26. Khatmi, G. et al. SPIE photonics europe, strasbourg, france,. laser micromachining for enhancing lateral flow assay colorimetric signal sensitivity. In *Proceedings Volume 13008, Biophotonics in Point-of-Care III; 130080 M (2024)* (eds. Michael T. Canva, Ambra Giannetti, Hatice Altug & Julien Moreau Editor Affiliations) 1–4. https://doi.org/10.1117/12.3012595 (2024).
27. Khatmi, G. et al. Self-contained microfluidic paper for Controlling Lateral Flow Assay Flow Rate with a Femtosecond Laser Micromachining, in *Frontiers in Optics + Laser Science 2023 (FiO, LS)*, Technical Digest Series (Optica Publishing Group, 2023), paper JTu5A.80. https://doi.org/10.1364/FIO.2023.JTu5A.80 (2023).
28. Gasperino, D., Baughman, T., Hsieh, H. V., Bell, D., & Weigl, B. H. Improving lateral flow assay performance using computational modeling. https://doi.org/10.1146/annurev-anchem-061417-125737 (2018).
29. Liang, T. et al. Investigation of reagent delivery formats in a multivalent malaria sandwich immunoassay and implications for assay performance. *Anal. Chem.* **88**, 2311–2320. https://doi.org/10.1021/acs.analchem.5b04222 (2016).
30. Quesada-González, D. et al. Signal enhancement on gold nanoparticle-based lateral flow tests using cellulose nanofibers. *Biosens. Bioelectron.* **141**. https://doi.org/10.1016/j.bios.2019.111407 (2019).
31. Adomavičiūtė, E. et al. Micro-structuring of electrospun mats employing femtosecond laser. *Medziagotyra*. **21**, 44–51. https://doi.org/10.5755/j01.ms.21.1.10249 (2015).
32. Skordoulis, C. D., Makropoulou, M. I. & Serafetinides, A. A. Ablative etching of nitrocellulose with infra-red and ultra-violet laser radiation. *Opt. Laser Technol.* 185–189. https://doi.org/10.1016/0030-3992(95)93639-9 (1995).
33. Pablo, J. & Urbina, C. *Efficient Material Laser Beam Ablation with a Picosecond Laser*. 978-3-662-61885-1. http://www.springer.com/series/13397 (2020).
34. Bastús, N. G., Comenge, J. & Puntes, V. Kinetically controlled seeded growth synthesis of citrate-stabilized gold nanoparticles of up to 200 nm: size focusing versus ostwald ripening. *Langmuir*. **27**, 11098–11105. https://doi.org/10.1021/la201938u (2011).
35. Park, S. B. & Shin, J. H. Pressed lateral Flow Assay Strips for Flow Delay-Induced Signal Enhancement in lateral Flow Assay Strips. *Biochip J.* **16**, 480–489. https://doi.org/10.1007/s13206-022-00085-w (2022).
36. Tang, R. et al. Improved Analytical sensitivity of lateral Flow assay using sponge for HBV Nucleic Acid Detection. *Sci. Rep.* **7**, 1360. https://doi.org/10.1038/s41598-017-01558-x (2017).
37. Sena-Torralba, A. et al. Lateral flow assay modified with time-delay wax barriers as a sensitivity and signal enhancement strategy. *Biosens. Bioelectron.* **168**. https://doi.org/10.1016/j.bios.2020.112559 (2020).
38. Xiao, Z., Yang, Y., Zhang, X. & Guo, W. Controlling capillary flow rate on lateral flow test substrates by tape. *Micromachines (Basel)*. **12**https://doi.org/10.3390/mi12050562 (2021).
39. Wang, X. et al. Evaporation-Induced Diffusion acceleration in liquid-filled porous materials. *ACS Omega*. **6**, 21646–21654. https://doi.org/10.1021/acsomega.1c03052 (2021).
40. Liu, Z., Hu, J., Zhao, Y., Qu, Z. & Xu, F. Experimental and numerical studies on liquid wicking into filter papers for paper-based diagnostics. *Appl. Therm. Eng.* **88**, 280–287. https://doi.org/10.1016/j.applthermaleng.2014.09.057 (2015).
41. Sun, S. et al. Microstructural effects on permeability of nitrocellulose membranes for biomedical applications. *J. Memb. Sci.* **595**. https://doi.org/10.1016/j.memsci.2019.117502 (2020).
42. Yetisen, A. K., Akram, M. S. & Lowe, C. R. Paper-based microfluidic point-of-care diagnostic devices. *Lab. Chip*. **13**, 2210–2251. https://doi.org/10.1039/c3lc50169h (2013).
43. Antanavičiūtė, I. et al. Femtosecond laser micro-machined polyimide films for cell scaffold applications. *J. Tissue Eng. Regen Med.* **12**, e760–e773. https://doi.org/10.1002/term.2376 (2018).
44. Liu, J. M. Simple technique for measurements of pulsed gaussian-beam spot sizes. *Opt. Lett.* **7**, 196–198. https://doi.org/10.1364/OL.7.000196 (1982).
45. Sanner, N. et al. Measurement of femtosecond laser-induced damage and ablation thresholds in dielectrics. *Appl. Phys. A*. **94**, 889–897. https://doi.org/10.1007/s00339-009-5077-6 (2009).

Acknowledgements

Author contributions

Gazy Khatmi—investigation, formal analysis, visualization, writing—original draft preparation, writing—review, and editing. Tomas Klinavičius—methodology, writing—original draft preparation. Asta Tamulevičienė—investigation, writing—original draft preparation. Martynas Simanavičius—conceptualization, methodology, investigation, formal analysis, writing—review, and editing. Laimis Silimavičius—conceptualization, methodology, writing—review, and editing. Agnė Rimkutė—methodology, investigation, formal analysis. Indrė Kučinskaitė-Kodzė—methodology, investigation, formal analysis. Gintautas Gylys—conceptualization, methodology, project administration. Tomas Tamulevičius—conceptualization, visualization, methodology, resources, funding acquisition, project administration, writing—original draft preparation, writing—review, and editing.

Declarations

Competing interests

The authors declare no competing interests.

Additional information

Supplementary Information The online version contains supplementary material available at https://doi.org/10.1038/s41598-024-74407-3.

Correspondence and requests for materials should be addressed to G.K. or T.T.

Reprints and permissions information is available at www.nature.com/reprints.

Publisher's note Springer Nature remains neutral with regard to jurisdictional claims in published maps and institutional affiliations.